Available online at www.sciencedirect.com
SCIENCE DIRECT®
Journal of Power Sources 142 (2005) 200–210
JOURNAL OF POWER SOURCES
www.elsevier.com/locate/jpowsour

Non-destructive inverse method for determination of irregular internal temperature distribution in PEMFCs

Mei-Hsia Chang, Chin-Hsiang Cheng*

Department of Mechanical Engineering, Tatung University, 40 Chungshan N. Road, Sec. 3, Taipei 10451, Taiwan, ROC

Received 10 October 2004; accepted 1 November 2004
Available online 15 January 2005

Abstract

A non-destructive inverse method is developed to determine internal temperature distribution of the PEMFCs. In this study, the attention is focused on global measurement for the irregular temperature distribution at the interface between the carbon plate and the membrane electrode assembly (MEA) based on the measured temperature data on the outer surface of the end plate. A direct problem solver capable of predicting temperature distribution in the solid layers of the PEMFC under various conditions is incorporated in the inverse approach to provide temperature solutions. In this report, a concept of point-by-point temperature prediction is presented. This approach is particularly suitable for determining irregular temperature distribution that is difficult to handle by the existing polynomial-function approach [C.H. Cheng, M.H. Chang, Predictions of internal temperature distribution of PEMFC by undestructive inverse method, J. Power Sources, in press]. A number of test cases are considered in this study. Some irregular temperature functions are specified and regarded as exact temperature distributions to predict. Meanwhile, the influence of uncertainty in the measured temperature data on the outer surface is evaluated.

Keywords: Non-destructive measurement; Temperature prediction; PEMFC; Inverse method

1. Introduction

In the past several years, significant progress in the development of fuel cell technology has been achieved by an increasing number of experimental [1–3] and theoretical [4–7] studies. The experiments can help determine the overall performance of the fuel cell and find out preferable operation conditions. The theoretical studies help understand the physico-chemical process and the transportation phenomena inside the fuel cell and provide detailed information which may not be easily obtainable by the experiments.

On the other hand, the optimization methods are gradually introduced into the fuel cell design phase. For example, a nonlinear-constrained optimization procedure to maximize the performance of the cathode with interdigitated air channels in a PEMFC was presented by Grujicic et al. [8]. In Ref. [8], the optimization was based on a steady-state single-phase electro-chemical model for the cathode. In the study of Mohamed and Jenkins [9], a genetic algorithm is employed to optimize a PEMFC stack design by searching for the best configuration in terms of cell number and the cell surface area. Grujicic and Chittajallu [10] used a two-dimensional electrochemical model to determine the optimal design of the operational and the geometrical parameters for cathode of a fuel cell.

In general, the electrical energy produced is accompanied by an approximately equal amount of thermal energy dissipated. Therefore, thermal management of a fuel cell is of great concerns to the researchers. In order to ensure efficient thermal management for the fuel cell, it is required to monitor the internal temperature distribution of the PEMFC. However, the internal temperature of the fuel cell is usually not easily measured, especially for a global measurement. To have the internal temperature information, one may use destructive methods, in which a number of temperature sensors are inserted into the fuel cell to measure the internal temperature

* Corresponding author. Tel.: +886 2 25925252/3410; fax: +886 2 25997142.
E-mail address: cheng@ttu.edu.tw (C.-H. Cheng).

0378-7753/$ – see front matter © 2004 Elsevier B.V. All rights reserved.
doi:10.1016/j.jpowsour.2004.11.019

Nomenclature

C	heat capacity (kJ kg^{-1} °C^{-1})
h	heat transfer coefficient (W m^{-2} °C^{-1})
H	height (m)
J	objective function
k	thermal conductivity (W m^{-1} °C^{-1})
L	length of fuel cell (m)
NX, NY, NZ	numbers of grid points in x-, y-, and z-direction
q^*	internal heat source (W m^{-3})
t	time
T	temperature (°C)
$\overline{T}$	simulated experimental temperature data (°C)
T_a	ambient temperature (°C)
W	thickness (m)
x, y, z	Cartesian coordinates (m)

Greek symbols

β	step size
γ	conjugate gradient coefficient
θ	exact temperature solution
ρ	density (kg m^{-3})
σ	experimental temperature uncertainty
ω	random number varied −1 and 1

Subscripts

C	carbon plate
Cu	copper plate
e	end plate
ex	exact
g	gasket
i, j, k	grid point indices
ini	initial guess

Superscript

n	iteration step

directly. Unfortunately, the destructive methods may appreciably disturb the original flow and current fields inside the fuel cell, and may also be possible to cause leakage problems of the fuel and oxidant gases.

In order to resolve these problems, Cheng and Chang [11] introduced the concept of an inverse method for obtaining the global temperature distribution at the MEA/carbon plate interface in the PEMFC. This method is capable of predicting internal temperature distribution of a PEMFC efficiently based on the outer surface temperature data without causing any damage to the fuel cell. However, in the study, the temperature distribution of the predicted interface must be approximated by a polynomial function. As a result, if predicted temperature distribution cannot be cast into a form of a polynomial function accurately, there will exists a remarkable error in predictions. Thus, the flexibility of the inverse method is actually limited due to the polynomial-function assumption.

In the present study, the existing polynomial-function approach is modified and extended to the applications for a more flexible form of temperature distribution at the MEA/carbon plate interface. The temperature distribution is predicted by using a point-by-point concept which is not limited by the mathematical assumption with a polynomial-function form for the temperature distribution. Therefore, even an irregular temperature distribution at the MEA/carbon plate interface can be predicted accurately.

The validity of the present method is demonstrated by dealing with two cases of exact temperature function. In addition, the influence of the uncertainty in the measured temperature data on the outer surface of the end plate is evaluated. Relative performance of the present approach is demonstrated by a comparison with the existing method.

Fig. 1 shows the schematic of a typical single-cell PEMFC. The PEMFC shown in this figure is equipped with a polymer electrolyte at the center. The polymer electrolyte is sandwiched between two electrodes and two gas diffusion layers to form a MEA, which is placed between two carbon plates having machined groves that provide flow channels for fuel and oxidant individually. In addition, two copper current collectors are attached to the outer faces of the carbon plates to conduct the current. In general, the outer surfaces of the copper current collectors are insulated by gasket layers. The single cell is then compressed tightly by two end plates.

While the cell is in operation, a certain amount of heat is generated by the electrochemical reaction. The heat generated must be conducted toward the outer surfaces of the

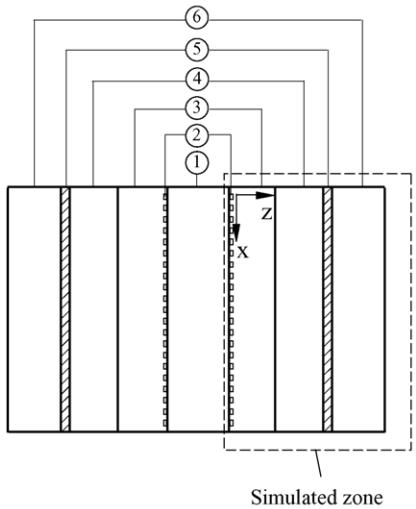

Fig. 1. Schematic of a single-cell PEMFC and the simulated zone.

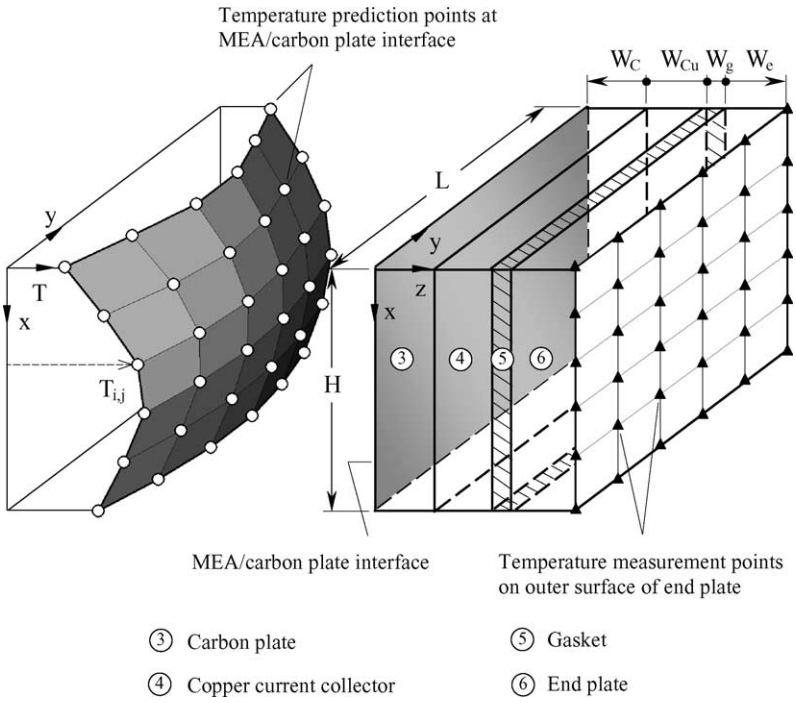

Fig. 2. Geometry of the simulated zone.

end plates and then dissipated to the ambient air at temperature T_a by convection. Heat transfer coefficient on the outer surfaces is denoted by h. As stated earlier, the temperature distribution at the MEA/carbon plate interface is predicted by the point-by-point approach based on the measured temperature data on the outer surface of the end plate. The temperature information on the outer surfaces of the end plates can be gathered by using an array of distributed temperature sensors installed on the outer surface of the end plate or by an infrared radiation thermal image system. Note that local temperature distribution at the MEA/carbon plate interface reflects local condition of electrochemical reaction to a certain extent. Since in the present study the MEA/carbon plate interface temperature is determined based on the temperature data on the outer surface of the end plate, the simulated zone is ranged from the MEA/carbon plate interface to the outer surface of the end plate, as indicated by the dashed lines in Fig. 1. Geometric variables of the simulated zone are illustrated in Fig. 2, and the fixed dimensions, material properties, and surface conditions are given in Table 1.

In Fig. 2, the array of the temperature measurement points on the outer surface of the end plate and the array of the temperature prediction points at the MEA/carbon plate interface are both shown. Typically, the numbers and the locations of the temperature measurement points, the temperature prediction points, and the grid points used in the numerical analysis of the direct problem solver, are all identical.

2. Optimization method

2.1. Direct problem solver

The solid materials in the simulated zone, including the carbon plate, copper current collector, gasket, and end plate of the PEMFC, are all assumed to be homogeneous, isotropic mediums. In these solid materials, heat conduction is governed by the following partial differential equation:

$$\rho C \frac{\partial T}{\partial t} = k\nabla^2 T + q^* \tag{1}$$

Table 1
Fixed dimensions, material properties, and surface conditions of the test cases

Carbon plate	Copper plate	Gasket	End plate
$L = 0.21$ m	$L = 0.21$ m	$L = 0.21$ m	$L = 0.21$ m
$W_C = 0.21$ m	$W_{Cu} = 0.21$ m	$W_g = 0.21$ m	$W_e = 0.21$ m
$H_C = 0.003$ m	$H_{Cu} = 0.003$ m	$H_g = 0.0003$ m	$H_e = 0.004$ m
$k_C = 95\,W\,m^{-1}\,{}^\circ C^{-1}$	$k_{Cu} = 380\,W\,m^{-1}\,{}^\circ C^{-1}$	$k_g = 0.17\,W\,m^{-1}\,{}^\circ C^{-1}$	$k_e = 200\,W\,m^{-1}\,{}^\circ C^{-1}$
Edge convection	Edge convection	Edge convection	Edge and outer surface convection
$h = 10\,W\,m^{-2}\,{}^\circ C^{-1}$	$h = 10\,W\,m^{-2}\,{}^\circ C^{-1}$	$h = 10\,W\,m^{-2}\,{}^\circ C^{-1}$	$h = 10\,W\,m^{-1}\,{}^\circ C^{-1}$
$T_a = 25\,{}^\circ C$	$T_a = 25\,{}^\circ C$	$T_a = 25\,{}^\circ C$	$T_a = 25\,{}^\circ C$

where q^* denotes the internal heat source; ρ, C, and k are density, heat capacity, and thermal conductivity of the individual solid materials, respectively; and T is the temperature. The present approach is based on the steady-state thermal behavior. Thus, the three-dimensional steady-state heat conduction equation without internal heat source can be derived as:

$$\frac{\partial^2 T}{\partial x^2} + \frac{\partial^2 T}{\partial y^2} + \frac{\partial^2 T}{\partial z^2} = 0 \tag{2}$$

The boundary conditions associated with the above heat conduction equation are:

(1) Outer surfaces of end plates or edges of all solid layers:

$$\pm k \frac{\partial T}{\partial n} = h[T - T_a] \tag{3a}$$

where n is the coordinate normal to the respective surfaces, and h is assigned to be $10\,\mathrm{W\,m^{-2}\,^\circ C^{-1}}$ for a natural-convection situation.

(2) Interfaces between two solids:

$$T_1 = T_2 \tag{3b}$$

$$k_1 \frac{\partial T_1}{\partial n_1} = k_2 \frac{\partial T_2}{\partial n_2} \tag{3c}$$

where the indices 1 and 2 denote the two successive solid layers in contact.

Eqs. (2) and (3) are then discretized to yield a set of simultaneous algebraic equations by the finite-difference method. With the help of successive-over-relaxation method (SOR) [12], the numerical solution for the three-dimensional temperature distribution at $NX \times NY \times NZ$ grid points can be obtained. Note that NZ is the sum of NZ_C, NZ_{Cu}, NZ_g, and NZ_e.

2.2. Inverse method

In the present study, an objective function (J) in conjunction with the optimization process is defined in the following:

$$J = \sum_{i=1}^{NX} \sum_{j=1}^{NY} (T_{ei,j} - \bar{T}_{ei,j})^2 \tag{4}$$

where $T_{ei,j}$ is the iterative temperature provided by the direct problem solver at the grid point (i, j) on the outer surface of the end plate, and $\bar{T}_{ei,j}$ is the experimental measurement temperature at the same point which is determined by $\bar{T}_{ei,j} = T_{ex\,i,j} + \sigma\omega$, where $T_{ex\,i,j}$, σ, and ω are the exact temperature, experimental uncertainty, and a random number varied -1 and 1, respectively. Note that when $\sigma = 0$, the experimental temperature distribution measured on the end plate is identical to the exact one. In addition, the MEA/carbon plate interface temperature distribution to predict, T_C (X, Y), is represented by a matrix of $NX \times NY$ discrete values of $T_{Ci,j}$. The $NX \times NY$ values of $T_{Ci,j}$ at the $NX \times NY$ grid points, that lead to minimization of the objective function defined in Eq. (4), are determined by using the optimization method. In other words, $T_{Ci,j}$ at all the $NX \times NY$ grid points at the MEA/carbon plate interface are regarded as the major variables to predict. Despite of longer computation time consumed, this point-by-point approach is capable of predicting interface temperature distribution corresponding to any sets of the measured temperature data.

Minimization of the objective function makes the difference between $T_{ei,j}$ and $\bar{T}_{ei,j}$ vanish. The minimization of the objective function J is achieved by using the conjugate-gradient method described by Hanke [13]. The conjugate-gradient method is used to evaluate the gradients of the objective function and to find the conjugate directions for the updated solutions with the help of a numerical sensitivity analysis proposed by Cheng and Wu [14]. In general, in a finite number of iterations the convergence can be attained.

In this study, the inverse method is further modified to become compatible with the point-by-point approach. For this purpose, let $T^n_{Ci,j}$ ($i = 1, 2, \ldots, NX$; $j = 1, 2, \ldots, NY$) be the nth iterative values of the temperature at grid point (i, j) at the interface between the carbon plate and MEA, and let the first search direction toward the minimization of J be the steepest descent direction in terms of the gradient functions

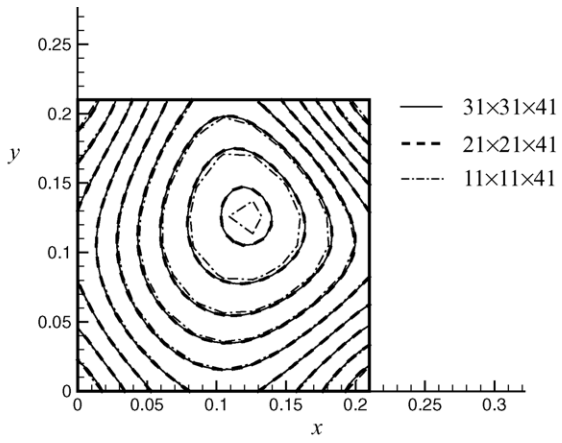

(a) Temperature distribution on plane at $z = 0.0015$ m

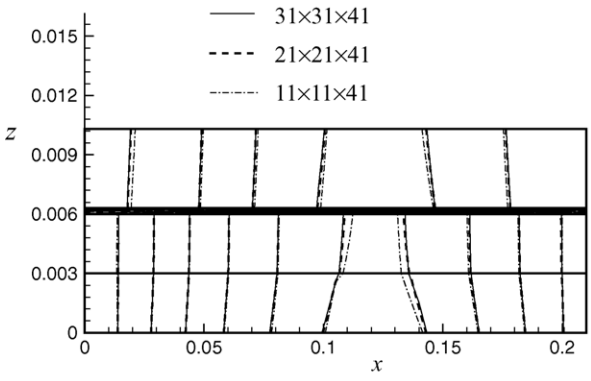

(b) Temperature distribution on plane at $y = 0.105$ m

Fig. 3. Grid independence of temperature solutions obtained by direct problem solver, based on $11 \times 11 \times 41$, $21 \times 21 \times 41$, and $31 \times 31 \times 41$ grids. The exact temperature function of case 2 is given for the MEA/carbon plate interface.

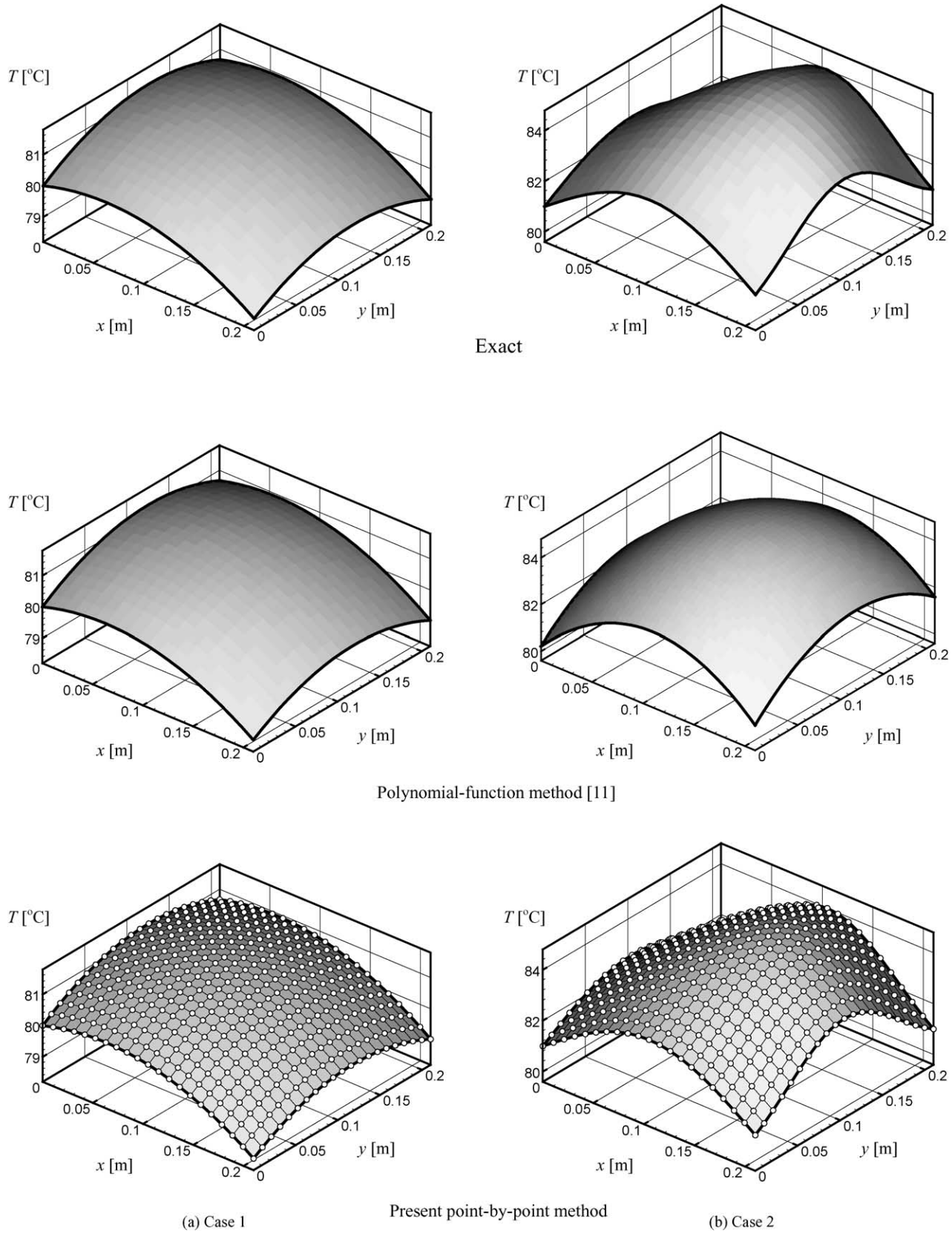

Fig. 4. Comparison between polynomial-function method [11] and present approach, for cases 1 and 2.

which are determined by

$$\frac{\partial J}{\partial T_{\mathrm{C}i,j}} = \sum_{k=1}^{NX}\sum_{q=1}^{NY} 2(T_{\mathrm{e}k,q} - \bar{T}_{\mathrm{e}k,q})\frac{\partial T_{\mathrm{e}k,q}}{\partial T_{\mathrm{C}i,j}},$$

$$i = 1, 2, \ldots, NX; \quad j = 1, 2, \ldots, NY \tag{5}$$

where the terms $\partial T_{\mathrm{e}k,q}/\partial T_{\mathrm{C}i,j}$ are referred to as the sensitivity coefficients. The task of the numerical sensitivity analysis [14] is to evaluate the sensitivity of the objective function J with respect to the perturbations of $T_{\mathrm{C}i,j}$. Therefore, the terms $\partial T_{\mathrm{e}k,q}/\partial T_{\mathrm{C}i,j}$ on the right-hand side of Eq. (5) are calculated by introducing small perturbations to $T_{\mathrm{C}i,j}$ at grid point (i, j) at the predicted interface. The perturbed temperature on the predicted interface is carried out, and then the three-dimensional temperature solutions are obtained by the direct problem solver. By using the obtained temperature solutions, the sensitivity of $T_{\mathrm{e}k,q}$ at point (k, q) to the perturbation in $T_{\mathrm{C}i,j}$ at point (i, j) is determined such that the value of $\partial T_{\mathrm{e}k,q}/\partial T_{\mathrm{C}i,j}$ can be calculated. The choice of the magnitude of the small perturbation in $T_{\mathrm{C}i,j}$ for each grid point at the MEA/carbon plate interface is critical for the numerical sensitivity analysis. In the study, the perturbation quantity is typically chosen between 0.1 and 1.0.

Based on the conjugate-gradient method, the values of $T_{\mathrm{C}i,j}$ on all the grid points are updated by

$$T^{n+1}_{\mathrm{C}i,j} = T^{n}_{\mathrm{C}i,j} - \beta_{i,j}\pi^{n}_{i,j},$$

$$i = 1, 2, \ldots, NX; \quad j = 1, 2, \ldots, NY \tag{6}$$

where each of the search directions $\pi^n_{i,j}$ is expressed as a linear combination of the steepest descent directions and a modified vector. That is,

$$\pi^{n}_{i,j} = \frac{\partial J}{\partial T_{\mathrm{C}i,j}} + \gamma^{n}_{i,j}\pi^{n-1}_{i,j},$$

$$i = 1, 2, \ldots, NX; \quad j = 1, 2, \ldots, NY \tag{7}$$

where the conjugate gradient coefficients $\gamma^n_{i,j}$ are calculated by

$$\gamma^{n}_{i,j} = \left[\frac{(\partial J/\partial T_{\mathrm{C}i,j})^{n}}{(\partial J/\partial T_{\mathrm{C}i,j})^{n-1}}\right]^2,$$

$$i = 1, 2, \ldots, NX; \quad j = 1, 2, \ldots, NY \tag{8}$$

The step sizes $\beta_{i,j}$ ($i = 1, 2, \ldots, NX$; $j = 1, 2, \ldots, NY$) appearing in Eq. (6) are to be determined. In theory, the values of $\beta_{i,j}$ are selected to minimize the updated objective function J^{n+1}. With the help of Eqs. (4) and (6), J^{n+1} can be deduced as

$$\begin{aligned} J^{n+1} &= \sum_{i=1}^{NX}\sum_{j=1}^{NY}[T^{n+1}_{\mathrm{e}i,j}(T^{n+1}_{\mathrm{C}1,1}, T^{n+1}_{\mathrm{C}1,2}, \ldots, T^{n+1}_{\mathrm{C}1,NY}, \ldots, T^{n+1}_{\mathrm{C}\,NX,1}, T^{n+1}_{\mathrm{C}\,NX,2}, \ldots, T^{n+1}_{\mathrm{C}\,NX,NY}) - \bar{T}_{\mathrm{e}i,j}]^2 \\ &= \sum_{i=1}^{NX}\sum_{j=1}^{NY}[T^{n+1}_{\mathrm{e}i,j}(T^{n}_{\mathrm{C}1,1} - \beta_{1,1}\pi^{n}_{1,1}, T^{n}_{\mathrm{C}1,2} - \beta_{1,2}\pi^{n}_{1,2}, \ldots, T^{n}_{\mathrm{C}1,NY} \\ &\quad -\beta_{1,NY}\pi^{n}_{1,NY}, \ldots, T^{n}_{\mathrm{C}\,NX,1} - \beta_{NX,1}\pi^{n}_{NX,1}, T^{n}_{\mathrm{C}\,NX,2} - \beta_{NX,2}\pi^{n}_{NX,2}, \ldots, T^{n}_{\mathrm{C}\,NX,NY} - \beta_{NX,NY}\pi^{n}_{NX,NY}) - \bar{T}_{\mathrm{e}i,j}]^2 \end{aligned} \tag{9}$$

By introducing a first-order Taylor series approximation into the above expression, the $(n+1)$th objective function becomes

$$\begin{aligned} J^{n+1} = \sum_{i=1}^{NX}\sum_{j=1}^{NY}\Bigg[(T^{n}_{\mathrm{e}i,j} - \bar{T}_{\mathrm{e}i,j}) - \Bigg(&\beta_{1,1}\pi^{n}_{1,1}\frac{\partial T^{n}_{\mathrm{e}i,j}}{\partial T^{n}_{\mathrm{C}1,1}} + \beta_{1,2}\pi^{n}_{1,2}\frac{\partial T^{n}_{\mathrm{e}i,j}}{\partial T^{n}_{\mathrm{C}1,2}} + \cdots + \beta_{1,NY}\pi^{n}_{1,NY}\frac{\partial T^{n}_{\mathrm{e}i,j}}{\partial T^{n}_{\mathrm{C}1,NY}} + \cdots \\ &+\beta_{NX,1}\pi^{n}_{NX,1}\frac{\partial T^{n}_{\mathrm{e}i,j}}{\partial T^{n}_{\mathrm{C}\,NX,1}} + \beta_{NX,2}\pi^{n}_{NX,2}\frac{\partial T^{n}_{\mathrm{e}i,j}}{\partial T^{n}_{\mathrm{C}\,NX,2}} + \cdots + \beta_{NX,NY}\pi^{n}_{NX,NY}\frac{\partial T^{n}_{\mathrm{e}i,j}}{\partial T^{n}_{\mathrm{C}\,NX,NY}}\Bigg)\Bigg]^2 \end{aligned} \tag{10}$$

Making the derivative of J^{n+1} with respect to $\beta_{i,j}$ vanish gives

$$\begin{aligned} &\beta_{1,1}\pi^{n}_{1,1}\sum_{i=1}^{NX}\sum_{j=1}^{NY}\left(\frac{\partial T^{n}_{\mathrm{e}i,j}}{\partial T^{n}_{\mathrm{C}1,1}}\frac{\partial T^{n}_{\mathrm{e}i,j}}{\partial T^{n}_{\mathrm{C}k,q}}\right) + \cdots + \beta_{1,NY}\pi^{n}_{1,NY}\sum_{i=1}^{NX}\sum_{j=1}^{NY}\left(\frac{\partial T^{n}_{\mathrm{e}i,j}}{\partial T^{n}_{\mathrm{C}1,NY}}\frac{\partial T^{n}_{\mathrm{e}i,j}}{\partial T^{n}_{\mathrm{C}k,q}}\right) + \cdots + \\ &\beta_{NX,1}\pi^{n}_{NX,1}\sum_{i=1}^{NX}\sum_{j=1}^{NY}\left(\frac{\partial T^{n}_{\mathrm{e}i,j}}{\partial T^{n}_{\mathrm{C}\,NX,1}}\frac{\partial T^{n}_{\mathrm{e}i,j}}{\partial T^{n}_{\mathrm{C}k,q}}\right) + \cdots + \beta_{NX,NY}\pi^{n}_{NX,NY}\sum_{i=1}^{NX}\sum_{j=1}^{NY}\left(\frac{\partial T^{n}_{\mathrm{e}i,j}}{\partial T^{n}_{\mathrm{C}\,NX,NY}}\frac{\partial T^{n}_{\mathrm{e}i,j}}{\partial T^{n}_{\mathrm{C}k,q}}\right) \\ &= \sum_{i=1}^{NX}\sum_{j=1}^{NY}(T_{\mathrm{e}i,j} - \bar{T}_{\mathrm{e}i,j})\frac{\partial T^{n}_{\mathrm{e}i,j}}{\partial T^{n}_{\mathrm{C}k,q}}, \quad k = 1, 2, \ldots, NX; \quad q = 1, 2, \ldots, NY \end{aligned} \tag{11}$$

Eq. (11) represents a set of $NX \times NY$ linear algebraic equations which could be solved simultaneously to yield the optimal step size $\beta_{i,j}$ ($i = 1, 2, \ldots, NX$; $j = 1, 2, \ldots, NY$) for each $T_{Ci,j}$ at point (i, j). The solution can be evaluated numerically by means of the Gaussian elimination method or other similar solvers.

Based on the above method, the temperature distribution at the MEA/carbon plate interface, $T_{Ci,j}$, is updated in iteration until an optimal temperature distribution satisfying the J-minimization criterion is obtained. Typically, the J-minimization criterion of the temperature prediction is set with $J < 1.0 \times 10^{-5}$.

Two cases of known temperature distribution functions at the MEA/carbon plate interface are specified as the exact temperature solutions. For comparison, both the present approach and the existing approach [11] are applied to evaluate the relative performance of the present method. The two exact temperature functions, θ (x, y), are given as:

$$\text{Case 1}: \quad \theta(x, y) = 80 + 10x - 80x^2 + 20y - 80y^2 - 5xy \tag{12}$$

$$\text{Case 2}: \quad \theta(x, y) = \left[\sin\left(\frac{xy\pi}{LW}\right)\right]^2 + 2\sin\left(\frac{x\pi}{L}\right) + 1.5\sin\left(\frac{y\pi}{W}\right) + 81 \tag{13}$$

where θ is in °C and x and y are in m.

Firstly, numerical checks have been performed to ensure grid-independence of the direct problem solver. Numerical predictions of the three-dimensional temperature distribution in the PEMFC are obtained based on three different grid systems, and the obtained results are compared. Three grid systems, having $NX \times NY \times NZ = 11 \times 11 \times 41$, $21 \times 21 \times 41$, and $31 \times 31 \times 41$ grids, respectively, are tested. For the thermal condition in which the MEA/carbon plate interface temperature is specified with the exact temperature function of case 2, the numerical temperature solutions on the planes at $z = 0.0015$ m and at $y = 0.105$ m are shown in Fig. 3. In the figure, it is found that an increase in grid number from $21 \times 21 \times 41$ to $31 \times 31 \times 41$ produces no appreciable differences between the two sets of solutions. Therefore, the grid system of $21 \times 21 \times 41$ grids is used in this study typically.

The two exact temperature functions defined in Eqs. (12) and (13) are introduced individually for the thermal boundary condition at the MEA/carbon plate interface to obtain the three-dimensional temperature solutions in the PEMFC by the direct problem solver. From the obtained numerical three-dimensional temperature solutions, the temperature solutions on the outer surface of the end plate are recorded and regarded as the exact temperature distribution on the end-plate surface ($T_{ex\,i,j}$). The exact temperature $T_{ex\,i,j}$ is added by $\sigma\omega$ to provide the simulated experimental data $T_{ei,j}$ which are required for testing the inverse approach, as indicated earlier. The inverse approach is acceptable only if the prediction of the MEA/carbon plate interface temperature distribution based on the simulated experimental temperature data is identical to the exact temperature function θ (x, y) specified.

3. Results and discussion

Fig. 4 shows the advantages of the present approach. In this figure, the predicted MEA/carbon plate interface temperature distributions by the present point-by-point method and by the polynomial-function method [11] are compared with the exact temperature functions. Plotted in the left port are the results for case 1, and the results for case 2 are plotted in the right portion. It can be observed that for case 1 of which the exact temperature function to predict is actually a polynomial function expressed by Eq. (12), both the polynomial-function and the present methods lead to the temperature solutions identical to the exact temperature function. However, for the irregular exact temperature function of case 2 given in Eq. (13), the polynomial-function method fails to provide accu-

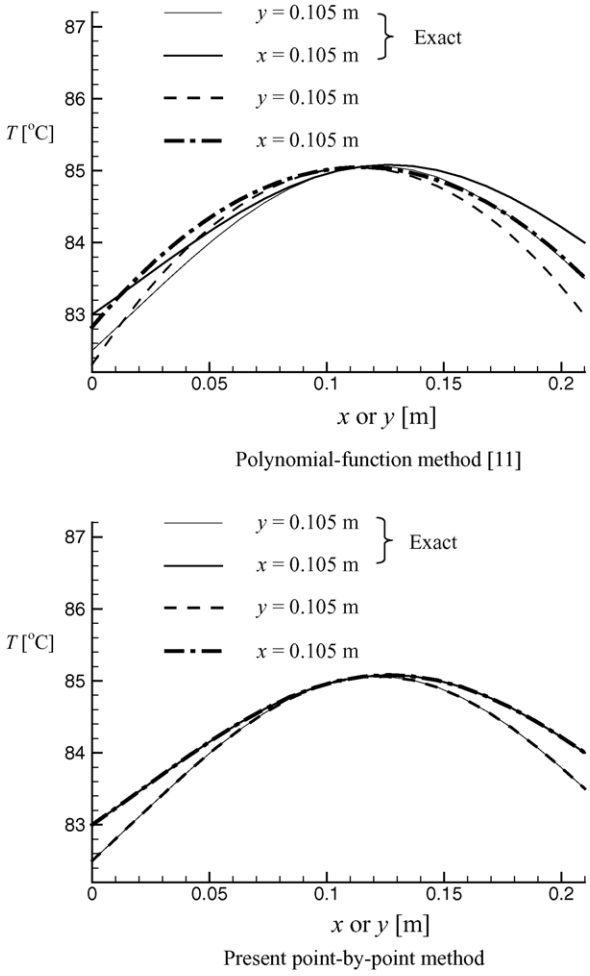

Fig. 5. Detailed temperature data along $x = 0.105$ m and $y = 0.105$ m: comparison between polynomial-function method [11] and present approach, for case 2.

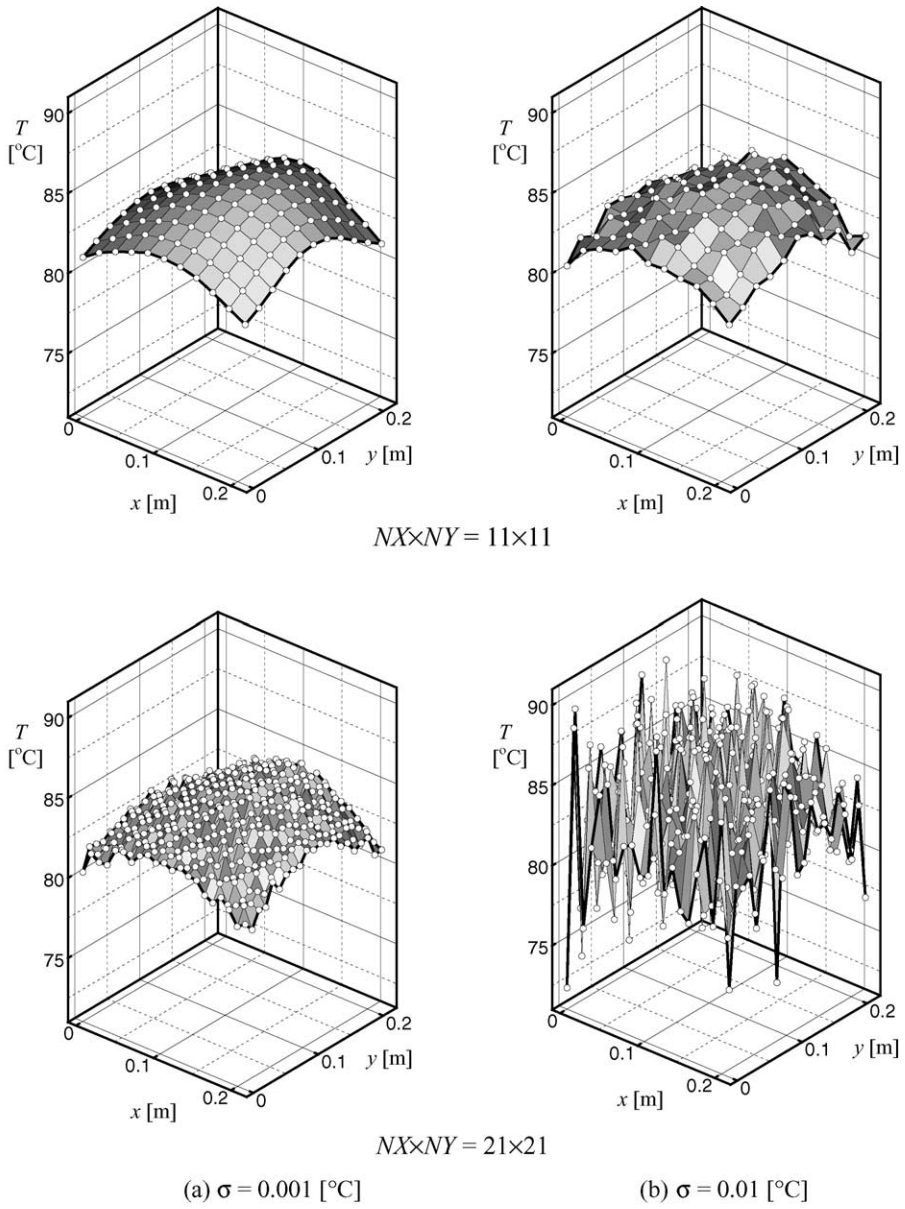

Fig. 6. Effects of experimental temperature uncertainty and number of temperature prediction points on predictions of temperature distribution at MEA/carbon plate interface.

rate predictions. Nevertheless, on the other hand, the present approach still leads to a satisfactory temperature distribution which closely agrees with the exact temperature function.

In order to have a closer look at the discrepancy between the two sets of results obtained by the two approaches, the predicted temperature profiles along the central line at $x = 0.105$ m and the central line at $y = 0.105$ m are plotted and compared with the exact profiles for case 2 (Fig. 5). The results obtained by the polynomial-function method are shown in the upper plot, and the results by the present approach in the lower plot. The dashed and dash-dot curves indicates the predicted solutions along $x = 0.105$ m and $y = 0.105$ m, respectively. The corresponding exact profiles are indicated by the solid and the thicker-solid curves. It is clearly observed that for this case the polynomial-function method produces significant errors in the predictions, while the present approach leads to satisfaction.

It is suspected that the uncertainty (σ) of the simulated experimental temperature data ($\overline{T}_{\mathrm{e}i,j}$) may play an important role in the accuracy of the solution. Meanwhile, the number of the temperature prediction points ($NX \times NY$) on the end plate surface may also be an influential factor. Fig. 6 shows the effects of uncertainty and number of prediction points on predictions of temperature distribution at MEA/carbon plate interface. It is found that the error of predictions is sensitive to the measurement uncertainty, and the relation between the prediction error and the measurement uncertainty is dependent on the number of prediction points. When 11×11

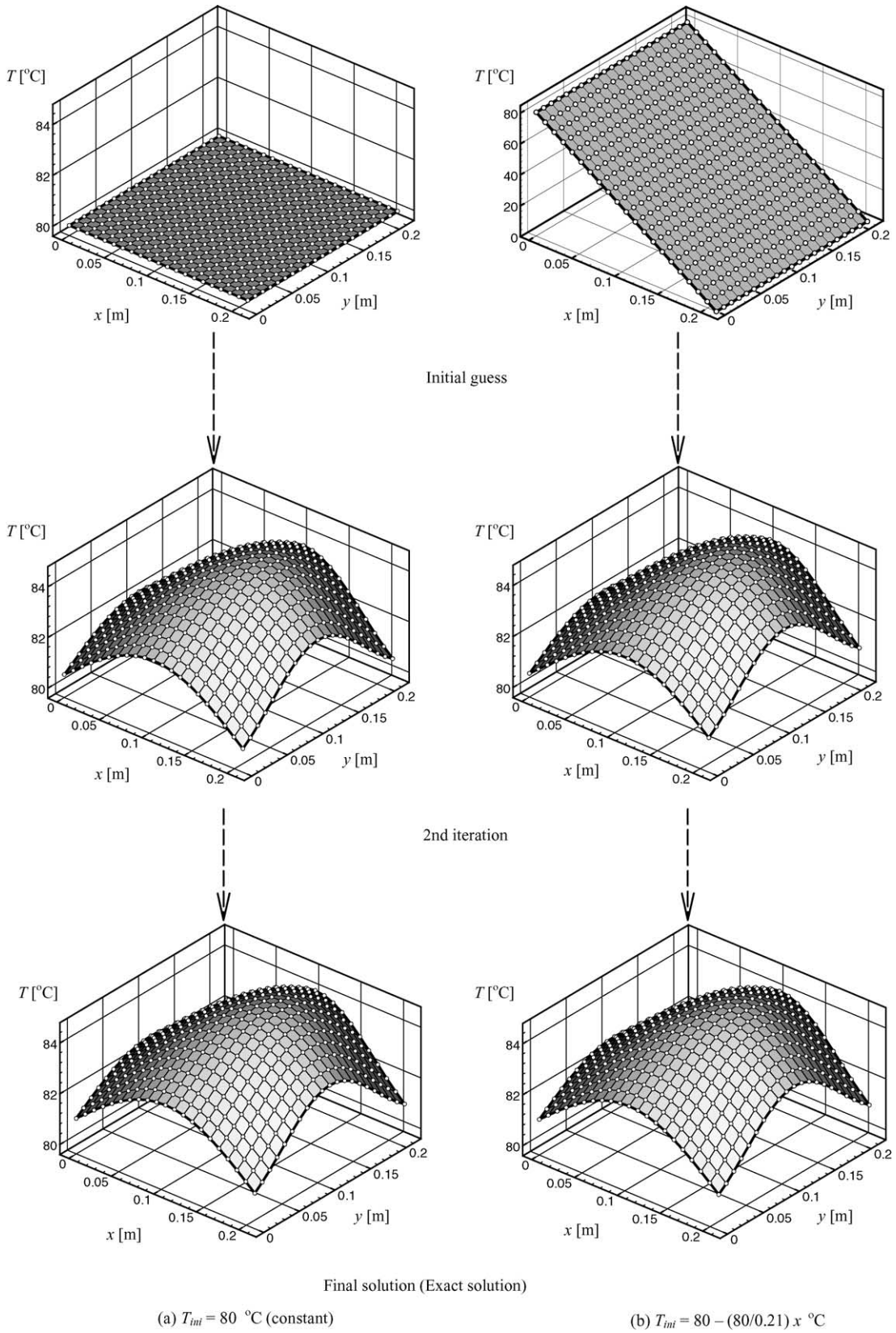

Fig. 7. Effects of initial guess on the final solution, for case 2.

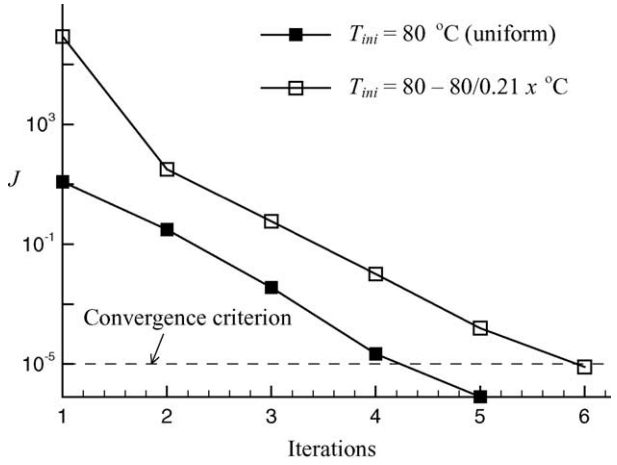

Fig. 8. Iterating objective functions with different initial guesses, for case 2.

prediction points are used, an uncertainty of 0.001 °C in simulated experimental data causes no appreciable prediction error. As σ is elevated to be 0.01 °C, the average fluctuation of the temperature predictions for the MEA/carbon plate interface is only increased to approximately 0.24 °C. However, when 21×21 prediction points are used, the fluctuation of the predictions becomes severer. The average value of the fluctuation reaches 2.26 °C at σ = 0.01 °C, which is not acceptable in practical applications. The increase in prediction error with the number of prediction points is expectable in the present approach since in this point-by-point approach, temperature at all the $NX \times NY$ prediction points on the MEA/carbon plate interface ($T_{Ci,j}$) are regarded as the major variables to predict. A larger number of the prediction points means a larger group of the major variables, and therefore, results in difficulties in reducing the magnitudes of the prediction errors. To improve the performance of the present approach, the fluctuation of the temperature predictions must be further reduced in future works.

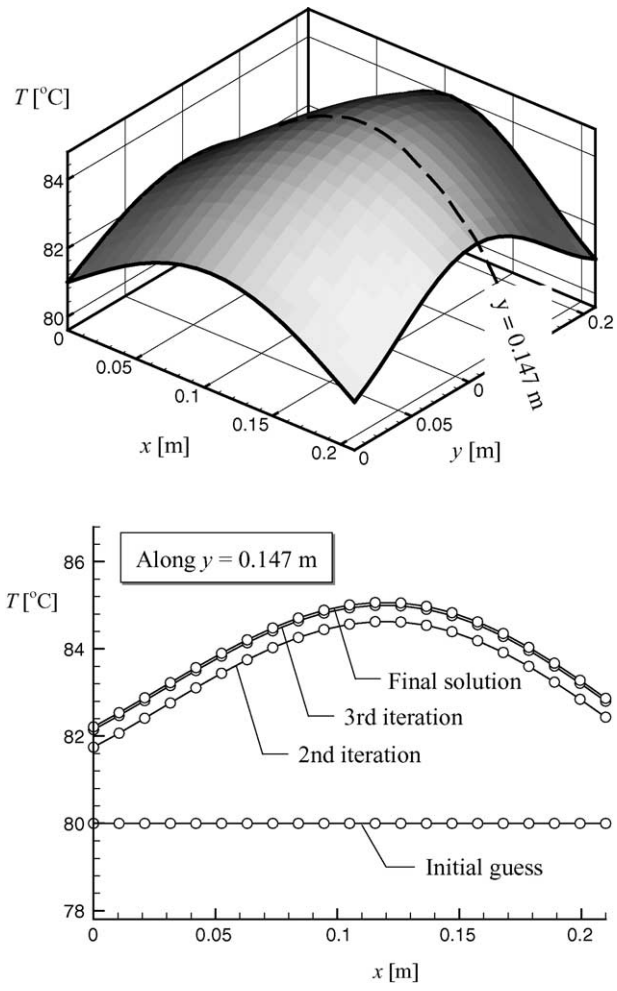

Fig. 9. Variation in temperature profile along the central line at y = 0.147 m, for initial guess of T_{ini} = 80 °C.

One may have reasons to suspect that the point-by-point method might not lead to unique solution when different initial guesses are used. To test the uniqueness of the predictions, two kinds of initial guess are adopted. One is a uniform temperature distribution, T_{ini} = 80 °C, and the other is a linearly-varied distribution from 0 to 80 °C given with $T_{ini} = 80 - (80/0.21)\,x$ °C. Fig. 7 shows the predicted temperature distributions yielded from the two different initial guesses by the present approach for case 2. It is interesting to find that for this case only one unique solution is obtained regardless of the initial guesses, and both the obtained solutions are in good agreement with the exact function. The associated objective functions varying with iteration step are shown in Fig. 8. The convergence criterion is set with $J < 1 \times 10^{-5}$. It is observed that the objective functions are decreased rather rapidly. The objective function of the test case with the initial guess of linearly varied temperature distribution is generally greater than that the uniform temperature distribution; however, in five to six iteration steps, both cases achieve convergence and lead to identical solutions by using the conjugate-gradient method. For the test case with the initial guess of uniform temperature distribution, the variation in temperature profile along the central line at y = 0.147 m is illustrated in Fig. 9. It is observed that the temperature profile is changed immediately to a profile which is close to the final solution at just the second iteration step. Then, in a few iterations the solution is rapidly improved to the one satisfying the convergence criterion.

4. Concluding remarks

A non-destructive inverse method is developed to determine internal global temperature distribution at the MEA/carbon plate interface in PEMFCs based on the measured temperature data on the outer surface of the end plate. A concept of point-by-point temperature prediction is presented and demonstrated by a number of test cases. Some irregular temperature functions are specified and regarded as exact temperature distributions to predict. Meanwhile, the influence of uncertainty in the measured temperature data on

the outer surface is evaluated. Relative performance of the present approach is demonstrated by a comparison with the polynomial-function method proposed by Cheng and Chang [11] in predicting the exact temperature distributions.

It is observed that for case 1 of which the exact temperature function to predict is actually a polynomial function, both the polynomial-function and the present methods lead to the temperature solutions identical to the exact temperature function. However, for the irregular exact temperature function of case 2, the polynomial-function method produces significant errors in the predictions, while the present approach leads to satisfaction.

The uncertainty (σ) of the simulated experimental temperature data ($\bar{T}_{ei,j}$) and the number of the temperature prediction points ($NX \times NY$) on the end plate surface are influential factor in the accuracy of the solution. It is found that the error of predictions is sensitive to the measurement uncertainty, and the relation between the prediction error and the measurement uncertainty is dependent on the number of prediction points. The prediction error increases with the measurement uncertainty or the number of prediction points.

Effects of the initial guess on the uniqueness of the predicted solution are investigated. It is found that for case 2 only one unique solution is obtained regardless of the initial guesses, and the obtained solutions from different initial guesses are in good agreement with the exact function.

References

[1] Y.G. Yoon, W.Y. Lee, T.H. Yang, G.G. Park, C.S. Kim, Current distribution in a single cell of PEMFC, J. Power Sources 118 (2003) 193–199.

[2] P.J.S. Vie, S. Kjelstrup, Thermal conductivities from temperature profiles in the polymer electrolyte fuel cell, Electrochim. Acta 49 (2004) 1069–1077.

[3] L.R. Jordan, A.K. Shukla, T. Behrsing, N.R. Avery, B.C. Muddle, M. Forsyth, Diffusion layer parameters influencing optimal fuel cell performance, J. Power Sources 86 (2000) 250–254.

[4] L. You, H. Liu, A two-phase flow and transport model for the cathode of PEM fuel cells, Int. J. Heat Mass Transfer 45 (2002) 2277–2287.

[5] D. Natarajan, T.V. Nguyen, Three-dimensional effects of liquid water flooding in the cathode of a PEM, Fuel Cell 115 (2003) 66–80.

[6] S. Dutta, S. Shimpalee, J.W.V. Zee, Numerical prediction of mass-exchange between cathode and anode channels in a PEM, Fuel Cell 44 (2001) 2029–2042.

[7] F. Chen, Y.G. Su, C.Y. Soong, W.M. Yan, H.S. Chu, Transient behavior of water transport in the membrane, J. Electroanal. Chem. 566 (2004) 85–93.

[8] M. Grujicic, C.L. Zhao, K.M. Chittajallu, J.M. Ochterbeck, Cathode and interdigitated air distribution geometry optimization in polymer electrolyte membrane (PEM) fuel cells, Mater. Sci. Eng. B 108 (2004) 241–252.

[9] I. Mohamed, N. Jenkins, Proton exchange membrane (PEM) fuel cell stack configuration using genetic algorithms, J. Power Sources 131 (2004) 142–146.

[10] M. Grujicic, K.M. Chittajallu, Design and optimization of polymer electrolyte membrane (PEM) fuel cell, Appl. Surf. Sci. 227 (2004) 56–72.

[11] C.H. Cheng, M.H. Chang, Predictions of internal temperature distribution of PEMFC by undestructive inverse method, J. Power Sources 139 (2005) 115–125.

[12] P. Moin, Fundamentals of Engineering Numerical Analysis, Cambridge University Press, New York, 2001.

[13] M. Hanke, Conjugate Gradient Type Methods for Ill-Posed Problems, John Wiley & Sons, New York, 1995.

[14] C.H. Cheng, C.Y. Wu, An approach combining body-fitted grid generation and conjugate gradient methods for shape design in heat conduction problems, Numer. Heat Transfer, Part B 37 (2000) 69–83.